Special Issue

Multistimuli-Responsive [3]Dioxaphosphaferrocenophanes with Orthogonal Switches

Bernhard S. Birenheide,[a] Felix Krämer,[a] Lea Bayer,[a] Paul Mehlmann,[b] Fabian Dielmann,*[b] and Frank Breher*[a]

Abstract: Novel multistimuli-responsive phosphine ligands comprising a redox-active [3]dioxaphosphaferrocenophane backbone and a P-bound imidazolin-2-ylidenamino entity that allows switching by protonation are reported. Investigation of the corresponding metal complexes and their redox behaviour are reported and show the sensitivity of the system towards protonation and metal coordination. The experimental findings are supported by DFT calculations. Protonation and oxidation events are applied in Rh-catalysed hydrosilylations and demonstrate a remarkable influence on reactivity and/or selectivity.

In recent years, the development of stimuli-responsive ligands and their coordination chemistry has garnered significant interest from the scientific research community. One of the main goals of this scientific branch is the ability to control multiple catalytic processes with a single active molecule, of which the activity can be altered by applying stimuli in a specific order. Efforts in this direction have led to the development of systems, where an (ideally reversible) change of the ligating properties of the ligand can be induced by external stimuli such as irradiation with light, protonation or redox-switching.[1] The donating capabilities of such ligands can thus be significantly altered and are usually investigated by measurement of the Tolman electronic parameter (TEP).[2] Redox-active systems are most often based on ferrocenyl (Fc)-containing mono- or multidentate ligands. In this context, ferrocenyl-decorated phosphines, *N*-heterocyclic carbenes (NHCs) and mesoionic carbenes (MICs) usually show a TEP change of approximately 7.4–12.7 cm^{-1} upon oxidation of the ferrocene unit.[3–6] The ferrocene (Fc)-based oxidation/reduction not only "switches" the σ-donor and π-acceptor properties of the ligand itself, but can further influence the properties of a coordinated metal. Investigations on catalytically active systems based on such multimetallic complexes have shown that changes can significantly influence the activity of the catalysts as well as its selectivity. This has been demonstrated in a variety of reactions such as ring-opening polymerization,[7,8] hydroamination,[9,10] or hydrosilylation,[4,11] among others.[10b]

The ability to switch the ligating properties of a ligand by protonation can be achieved by introduction of a Brønsted-basic pendent group. The groups of Glorius and Dielmann synthesized such systems based on an anionic enolate-imidazolinylidene ligand[12] and imidazoline-2-ylidenaminophosphines (IAPs),[13] respectively (Figure 1). The enolate-imidazolinylidene-based system exhibits a TEP change of 14 cm^{-1}, while the IAPs show an increase of approximately 22 cm^{-1} per protonation step, allowing an increase of up to 43 cm^{-1} upon twofold protonation. Further examples for stimuli-responsive ligands include external triggers such as UV-light[14] or coordination events.[15]

With these recent developments on multifunctional ligands[16] in mind, our groups became interested in combining the properties of redox-active and proton-sensitive systems, as it has already been shown that phosphoramidites with a ferrocenyl backbone are chemically accessible.[17] This would potentially allow for orthogonal switching by different stimuli, thus giving chemists a new tool to adapt towards reaction conditions in redox-switchable catalysis.

The dioxaphosphaferrocenophane-based[18] title compounds **L1** and **L2** (Scheme 1) were obtained by treating the known 1,1′-ferrocenediol[19] and the corresponding imidazoline-2-ylidenamino dichlorophosphines (**L1**: R = *i*Pr, **L2**: R = Mes) as yellow air- and moisture-sensitive crystalline solids in 50 and 44% isolated yield, respectively (Scheme 1). The ^{31}P NMR signals are observed at 142 and 156 ppm for **L1** and **L2**, respectively, which is comparable to other [3]dioxaphosphaferrocenophanes.[10]

The molecular structures were determined and are shown in Figure 2. In comparison to other [3]dioxaphosphaferrocenophanes, the distances between the iron atom and the phosphorus atom are increased. The known compounds in

[a] *B. S. Birenheide, F. Krämer, L. Bayer, Prof. Dr. F. Breher*
Institute of Inorganic Chemistry, Division Molecular Chemistry
Karlsruhe Institute of Technology (KIT)
Engesserstr.15, 76131 Karlsruhe (Germany)
E-mail: breher@kit.edu

[b] *Dr. P. Mehlmann, Prof. Dr. F. Dielmann*
Department of General, Inorganic and Theoretical Chemistry
Division Molecular Chemistry, University of Innsbruck
Center for Chemistry and Biomedicine
Innrain 80–82, 6020 Innsbruck (Austria)
E-mail: Fabian.Dielmann@uibk.ac.at

Supporting information for this article is available on the WWW under https://doi.org/10.1002/chem.202101969

This manuscript is part of a Special Issue "Cooperative effects in heterometallic complexes".

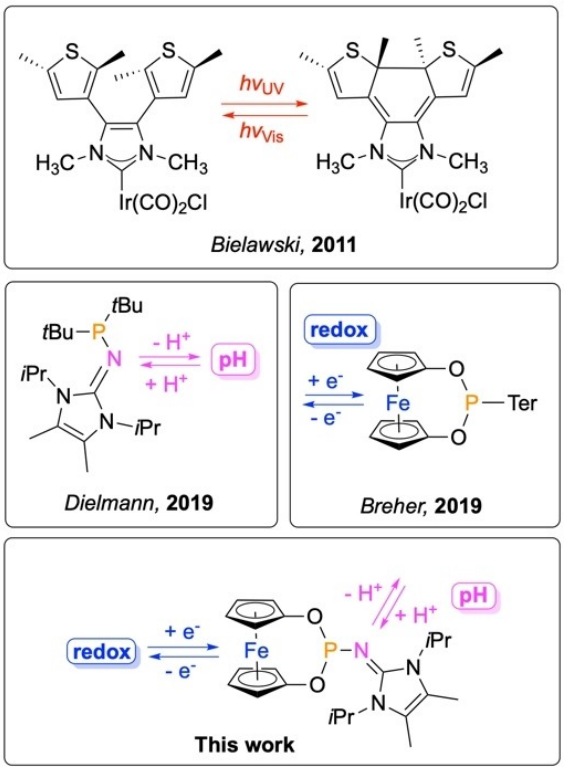

Figure 1. Examples of previously reported ligands and their switchability, as well as the targeted system of this work (Ter = terphenyl ligand).

which the phosphorus atom bears a *tert*-butyl- or a terphenyl-(2,6-$Mes_2C_6H_3$) moiety[10] show distances of $d = 330.8$ and 337.6 pm, respectively. For the proligands **L1** and **L2**, values of 343.7 and 358.7 pm, respectively, were found.

For direct measurement of the TEP values, and to compare the coordination behaviour of the ligands with previously reported phosphaferrocenophanes, we decided to focus on the synthesis of the corresponding Ni, Au and Rh compounds.

The metal complexes [**L1**Ni(CO)$_3$] (**1**), [**L1**AuCl] (**2**), and [**L1**Rh(cod)Cl] (**3**) for **L1** and [**L2**Ni(CO)$_3$] (**4**) and [**L2**Rh(cod)Cl] (**5**) for **L2** were prepared by reacting the free ligands with a suitable metal precursor in THF or toluene and were subsequently isolated by crystallization from concentrated *n*-hexane (**1** and **4**) or toluene (**2**, **3** and **5**) solutions (Scheme 2). Yields varied around 60% for the rhodium and gold compounds, while the nickel compounds could be obtained in almost quantitative yield.

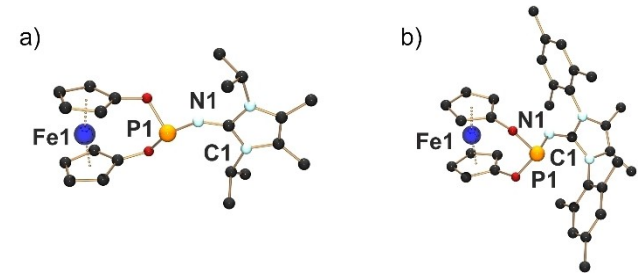

Figure 2. Molecular structures of a) **L1**[a] and b) **L2**. H atoms are omitted for clarity. Selected distances [pm]: **L1**: Fe1···P1 343.7, P1–N1 159.7; **L2**: Fe1···P1 358.7, P1–N1 163.9. [a] **L1** crystallizes with two molecules in the asymmetric unit. Distances are given as the average of both.

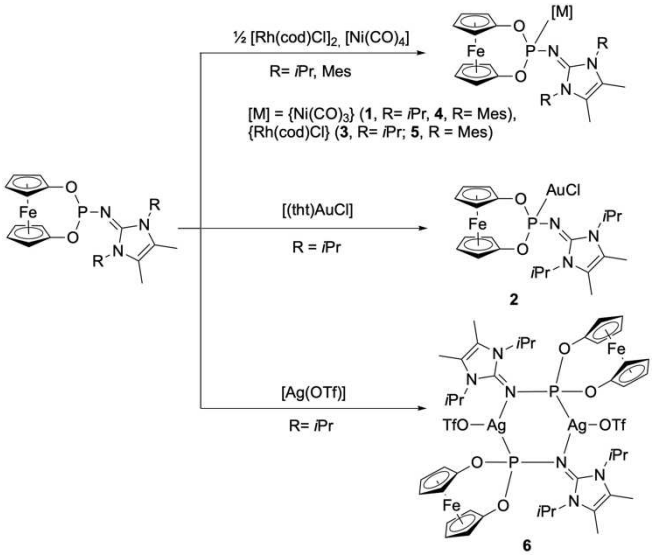

Scheme 2. Synthesis of compounds **1**–**6**.

Molecular structures of **1**–**5** were determined from single crystals and are shown in Figure 3. Whereas the distances in the ligand moiety of **L2** do not change significantly upon coordination of a metal fragment, a medium increase can be observed in the case of **L1**. Complexes **1** and **3** show a lengthening of the Fe···P distance of 11.3 and 11.8 pm, respectively. This is less pronounced in the gold(I) complex **2**, which can be explained by the steric demands of the coordinated metals, which is the lowest for **2**. However, compared to the other metal complexes of **L1**, the gold(I) complex shows a shortening of the P–N distance by 3.9 pm, and the N–C^{ipso} distance is lengthened by

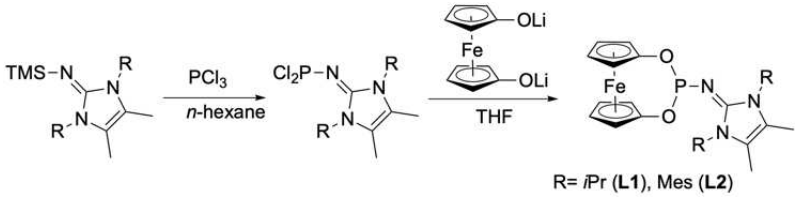

Scheme 1. Synthesis of **L1** and **L2**.

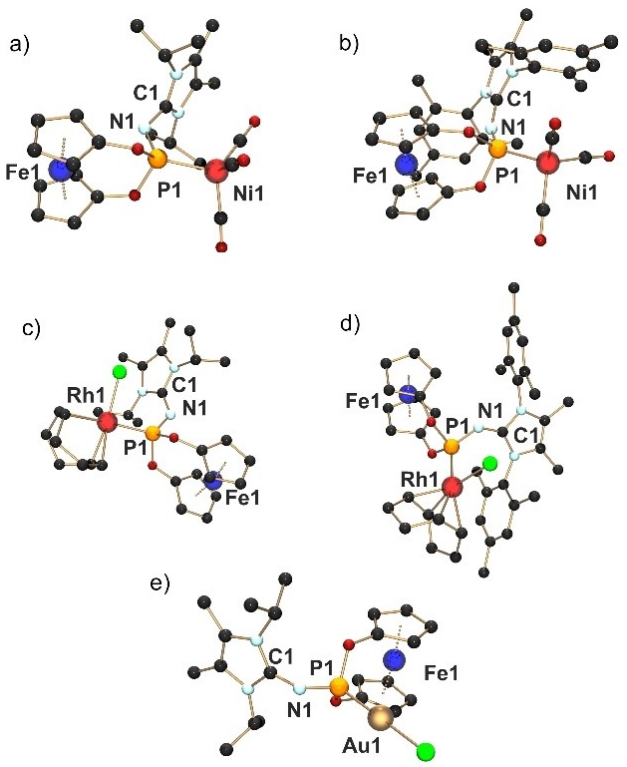

Figure 3. Molecular structures of a) [**L1**Ni(CO)$_3$] (**1**), b) [**L2**Ni(CO)$_3$] (**4**), c) [**L1**Rh(cod)Cl] (**3**), d) [**L2**Rh(cod)Cl] (**5**) and e) [**L1**AuCl] (**2**). H atoms are omitted for clarity. Selected distances and angles are given in Table 1.

4.3 pm. We believe that due to the high electron-withdrawing nature of the {AuCl} fragment more electron density is transferred from the phosphorus atom, thereby increasing the P–N bond strength, which in turn decreases the double bond character of the N–C^{ipso} bond.

While the proligands **L1** and **L2** behave relatively similar upon coordination, one significant difference can be observed. For metal complexes of **L1**, the M–P–N–C^{ipso} fragment is almost perfectly planar (Table 1), with the dihedral angle between the M–P–N and the P–N–C^{ipso} planes being between 0° and 7°. For metal complexes of **L2**, the torsion angle between the M–P–N and the P–N–C^{ipso} planes is around ~120°, with the imidazolium moiety sticking out of the M–P–N plane.

The TEP values of **L1** (2068.5 cm^{-1}) and **L2** (2064 cm^{-1}) were determined from the nickel(0) complexes **1** and **4**. The ligands are thus comparable with PPh_3 or PBz_3 and are better donors than the phosphite ligand P(O-^{i}Pr)$_2$Ph (TEP values of 2068, 2066 and 2072 cm^{-1}, respectively).[2]

Attempts to oxidize **L1** with AgOTf surprisingly yielded a dimeric compound (**6**, Figure 4), in which two ligands and two silver atoms form a six-membered ring. This structural motif represents an unusual coordination pattern for IAP-type ligands. The silver atoms are coordinated by one phosphorus atom, one nitrogen atom and the triflate ion. The metal complex does not appear to dissociate into monomeric units in solution, as can be deduced from the ^{31}P NMR spectrum. The doublets resulting from the $^1J(^{31}P–^{107}Ag)$ and $^1J(^{31}P–^{109}Ag)$ couplings are further split as result of the ^2J coupling to the second silver atom (Figure S30 in the Supporting Information).

Protonation of **L1** with [H(OEt$_2$)$_2$][Al(OC(CF$_3$)$_3$)$_4$] in THF furnished the protonated compound **L1H+**. In the crystal structure (Figure 5), hydrogen bonding of the N-bound proton towards one molecule of THF can be observed. The P–N and N–C^{ipso} distances are both increased by 7.8 and 6.6 pm, respectively, as compared to **L1** (Table 2). This is not surprising, as protonation decreases the electron density on the nitrogen atom, which in turn leads to a weakening of the aforementioned bonds.

The ^{1}H NMR spectrum of **L1H+** in [D$_8$]THF shows signals for two isomers clearly visible by two sets for the isopropyl C–*H* group, the ratio of which are roughly 3:1. We believe that this arises from coordination and de-coordination of the THF moiety and does not indicate decomposition as the ratio does not change even after several weeks. When protonation was carried out in situ in an NMR test tube, at first only the major isomer could be observed. The minor isomer formed over the course of three days after which the ratio does not change anymore. Furthermore, after addition of DBU, both signals for the isopropyl C–*H* group disappear and only one set corresponding to the deprotonated free proligand **L1** can be observed.

Table 2. Selected distances [pm] and angles [°] of **L1**, **2**, **L1H+** and **2H+**.

	d(Fe···P)	*d*(P–N)	*d*(N–C^{ipso})	*d*(P–M)	$\|\omega\|$(M–P–N– C^{ipso})
L1[a]	343.7	159.7	131.1	–	–
L1H+	339.0	167.5	137.7	–	–
2	347.8	155.8	135.4	221.2	0
2H+	340.0	162.1	141.5	219.7	1.0

[a] Averages of two molecules in the asymmetric unit.

Table 1. Selected distances [pm] and angles of **L1**, **L2** and **1**–**5**.

	d(Fe···P)	*d*(P–N)	*d*(N–C^{ipso})	*d*(P–M)	$\|\omega\|$(M–P–N– C^{ipso})
L1[a]	343.7	159.7	131.1	–	–
L2	358.7	163.9	129.9	–	–
[**L1**Rh(cod)Cl] (**3**)	355.5	159.6	132.7	224.8	7.0
[**L2**Rh(cod)Cl] (**5**)	354.8	160.3	130.1	225.8	123.3
[**L1**Ni(CO)$_3$] (**1**)[b]	355.0	160.3	133.4	219.1	5.0
[**L2**Ni(CO)$_3$] (**4**)	357.7	161.5	129.7	220.6	119.6
[**L1**AuCl] (**2**)	347.8	155.8	135.4	221.2	0

[a] Averages of two molecules in the asymmetric unit. [b] Averages of three molecules in the asymmetric unit.

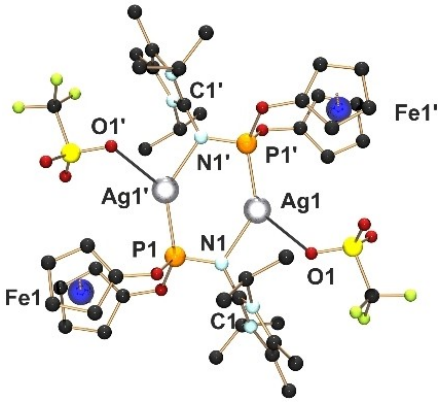

Figure 4. Molecular structure of **6**. H atoms and a co-crystallized molecule of CH_2Cl_2 are omitted for clarity. Selected distances [pm]: **L1**: Fe1···P1 344.5, P1–N1 161.0; P1–Ag1 236.2, N1–Ag1′ 224.0, Ag1–O1 240.2, Ag1···Ag1′ 325.7, N1–C1 136.9.

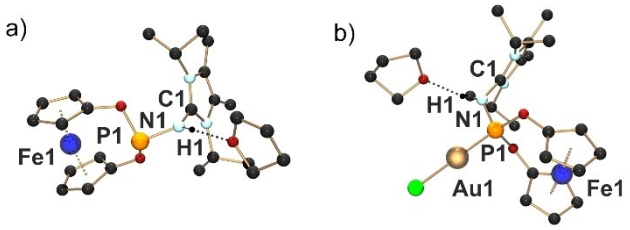

Figure 5. Molecular structures of a) the protonated proligand **L1H+** and b) the protonated gold(I) complex **2H+**. H atoms, co-crystallized solvents and counterions are omitted for clarity with the exception of the proton on the nitrogen atom N1. Selected distances and angles are given in Table 2.

The protonated gold(I) complex **2H+** can be prepared by treating **L1H+** with [(tht)AuCl] or by protonating **2** with $[H(OEt_2)_2][Al(OC(CF_3)_3)_4]$ (Scheme 3; isolated yields: 62% and 95% respectively). Similarly to **L1H+**, the proton is again engaged in a hydrogen bond with the oxygen atom of THF (Figure 5). The P–N and N–C^{ipso} distances increase by 6.3 pm and 6.1 pm, respectively, which underlines the effects observed for **L1H+**. Furthermore, the Fe···P distance decreases by 7.8 to 340 pm, which is comparable to the previously investigated gold(I) complexes of [3]dioxaphosphaferrocenophanes.[10]

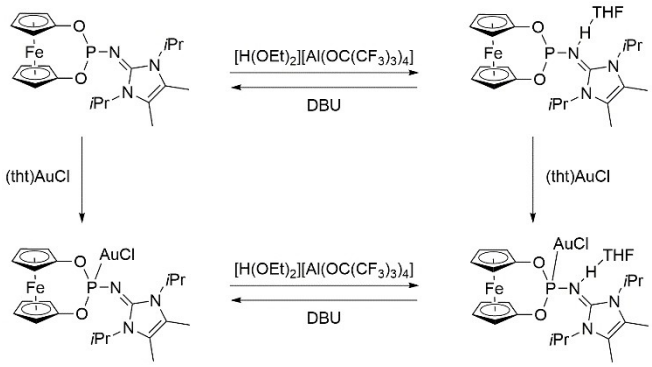

Scheme 3. Reaction pathways to the protonated proligand **L1H+** and the protonated gold(I) complex **2H+** (DBU = 1,8-Diazabicyclo[5.4.0]undec-7-ene).

In THF solution, the ^{1}H NMR spectrum shows only one set of signals even after several days, thus indicating that only one isomer is present. In contrast to all other compounds investigated, the protons of the methyl moieties in the imidazolyl residue are no longer equal and can be observed as two singlets; this shows that free rotation around the P–N or N–C^{ipso} bonds is hindered.

In situ protonation of nickel tricarbonyl complex **1** to furnish **1H+** gives a TEP of 2092 cm^{-1} with an increase of $\Delta TEP = +23.5\ cm^{-1}$ as compared to **1**. These observations are similar to the results of the protonation of IAPs, which led to an increase of $\Delta TEP = +22.5\ cm^{-1}$.[13] However, further characterization of protonated **1H+** was not possible due to fast decomposition in solution.

Protonation of **L2** and, independently, its nickel complex **4** also lead to decomposition, which can be observed by the disappearance of the CO bands in the IR spectrum. We believe that this can be attributed to the greater steric hinderance on the nitrogen atom. As the proton is bound to one or two molecules of the ethereal solvent, the imino group is far less accessible than the phosphinate group, which might give rise to protonation of the less robust O–P–O moiety.

The redox behaviour of the phosphaferrocenophanes and their metal complexes were investigated with the aid of cyclic voltammetry (Table 3, Figure 6). The $E^0_{1/2}$ values for the Fc-centred oxidation (see below) strongly depend on the coordinated transition metal fragment and/or the protonation of the ligand. The redox potential of the free ligands ($E^0_{1/2} = -160$ mV (**L1**) and −150 mV (**L2**) vs. Fc/Fc^+ in CH_2Cl_2) are cathodically shifted by approximately 150–200 mV in comparison to other [3]-dioxaphosphaferrocenophanes,[17] confirming the electron donating capabilities of the imidazolin-2-ylidenamino moiety. Coordination of a {AuCl} fragment (**2**, entry 5) leads to an anodic shift of +350 mV, which is slightly more pronounced as compared to previous studies from our laboratory[10] showing coordination shifts for {AuCl} complexes of about +270–300 mV. Protonation also has a dramatic influence on the redox potential of the ferrocene moiety (Entries 2 and 6). For the protonated free ligand **L1H+**, the redox potential is shifted by

Table 3. Half-wave potentials, peak potential differences and corresponding i_{pc}/i_{pa} values of the synthesized ligands and metal complexes in CH_2Cl_2 (THF) vs. Fc/Fc^+(internal standard Fc^*/Fc^{*+} or Fc/Fc^+, Fc* = decamethyl ferrocene; conditions: Pt/$[NBu_4][Al\{OC(CF_3)_3\}_4]$/Ag, $v = 100$ mV/s).

Compound	$E^0_{1/2}$ [mV]	ΔE_p [mV]	i_{pc}/i_{pa}	ΔE [mV] vs. **L1**
L2[a]	−160	120	~1	−10
L1[b]	−150 (−60)	250 (170)	~0.5[c] (~1)	0
[**L1**Ni(CO)$_3$] (**1**)	−80	220	~0.9	+70
[**L1**Rh(cod)Cl] (**3**)	−40	100	~1	+110
[**L1**AuCl] (**2**)	+200	150	~1	+350
L1H+	+390	120	~1	+540
[**L1**Ni(CO)$_3$H]$^+$	+480	220	~1	+630

[a] $[NBu_4][PF_6]$ was used as the electrolyte. [b] Quasi-reversible in CH_2Cl_2, fully reversible in THF. [c] $v = 500$ mV/s.

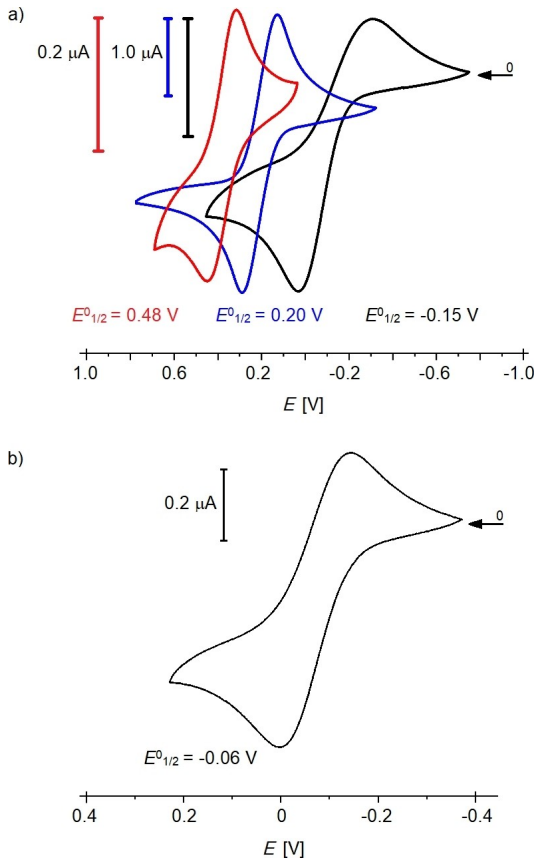

Figure 6. Cyclic voltammograms of a) **L1** (black), **2** (blue), and **L1H+** (red) in CH_2Cl_2 vs. Fc/Fc^+ and of b) **L1** in THF vs. Fc/Fc^+. Electrolyte: 0.01 M $[NBu_4][Al\{OC(CF_3)_3\}_4]$, v = 100 mV/s (500 mV/s for **L1** in CH_2Cl_2).

+540 mV as compared to **L1**. This observation is further supported by density functional theory (DFT) calculations at the B3LYP/def-2-TZVP level of theory. Compared to **L1**, the energies of the iron-centred HOMO is lowered by −0.3559 eV for the $\{Ni(CO)_3\}$ complex **1**. The experimental redox potential shift was found to be $\Delta E_{exp} = +70$ mV (entries 2 and 3). For the protonated ligand **L1H+**, a lowering of the HOMO of −2.8734 eV was calculated, which would translate into a calculated redox potential shift of about $\Delta E_{calc} = +560$ mV. Experimentally, a redox potential shift of $\Delta E_{exp} = +540$ mV was observed (entries 2 and 6). Similar redox potential shifts have been reported previously for ferrocene-based ligands upon coordination of monocationic metal ions, for instance.[20] In the

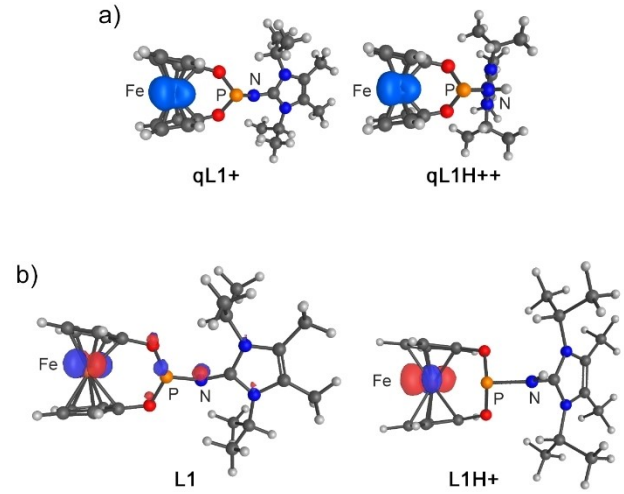

Figure 7. a) Calculated spin density of the oxidized proligands **qL1+** and **qL1H++**, iso value: 0.002. b) HOMOs of **L1** and **L1H+**, iso-value 0.075.

case of **L1**, the calculations also show, that while the HOMO is predominantly centred on the iron atom, a significant portion is also located on the nitrogen and phosphorus atoms, whereas in the case of **L1H+**, the HOMO is basically completely centred on the iron atom (Figure 7). Based on these findings we expected an additive effect upon coordination of a $\{Ni(CO)_3\}$ fragment ($\Delta E_{exp} = +70$ mV) and concomitant protonation ($\Delta E_{exp} = +540$ mV) to furnish a potential shift of about 610 mV. Indeed, cyclic voltammetry studies on $[\mathbf{L1}Ni(CO)_3H]^+$ gave $E^0_{1/2} = +480$ mV and, thus, $\Delta E_{exp} = +630$ mV against **L1**.

The effect of protonation on the redox potential can be observed by NMR spectroscopy (Scheme 4). Due to its lower redox potential than ferrocene, oxidation of **L1** with $[Cp_2Fe][B(C_6F_5)_4]$ leads to disappearance of the signals for **L1**, and only ferrocene can be observed in the ^1H NMR spectrum. However, since the protonated proligand **L1H+** is harder to oxidize than ferrocene, after addition of $[H(OEt_2)_2][Al(OC(CF_3)_3)_4]$, the ferrocene signal at $\delta_{1H} = 4.0$ ppm disappears again and signals corresponding to **L1H+** appear (Scheme 4).

Attempts to isolate the oxidized ligands and metal complexes always gave reddish-brown, paramagnetic oils, no matter the chosen oxidant or counterion. However, reacting **1** with a substoichiometric amount of $[CpFe(C_5H_4OMe)][PF_6]$ gave rise to a new CO band in the IR spectrum. The latter is observed at 2089 cm^{-1} (Figure S54), indicating a change of the TEP by

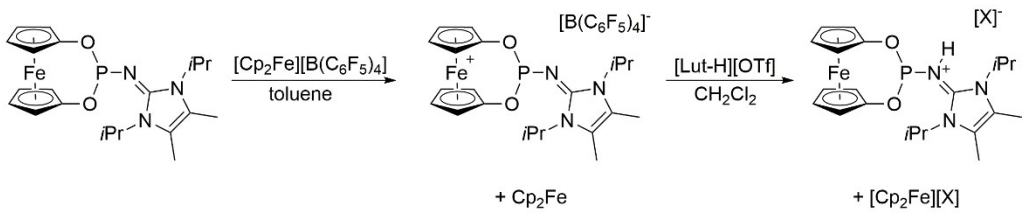

Scheme 4. NMR experiments on the sequential oxidation/protonation of **L1**.

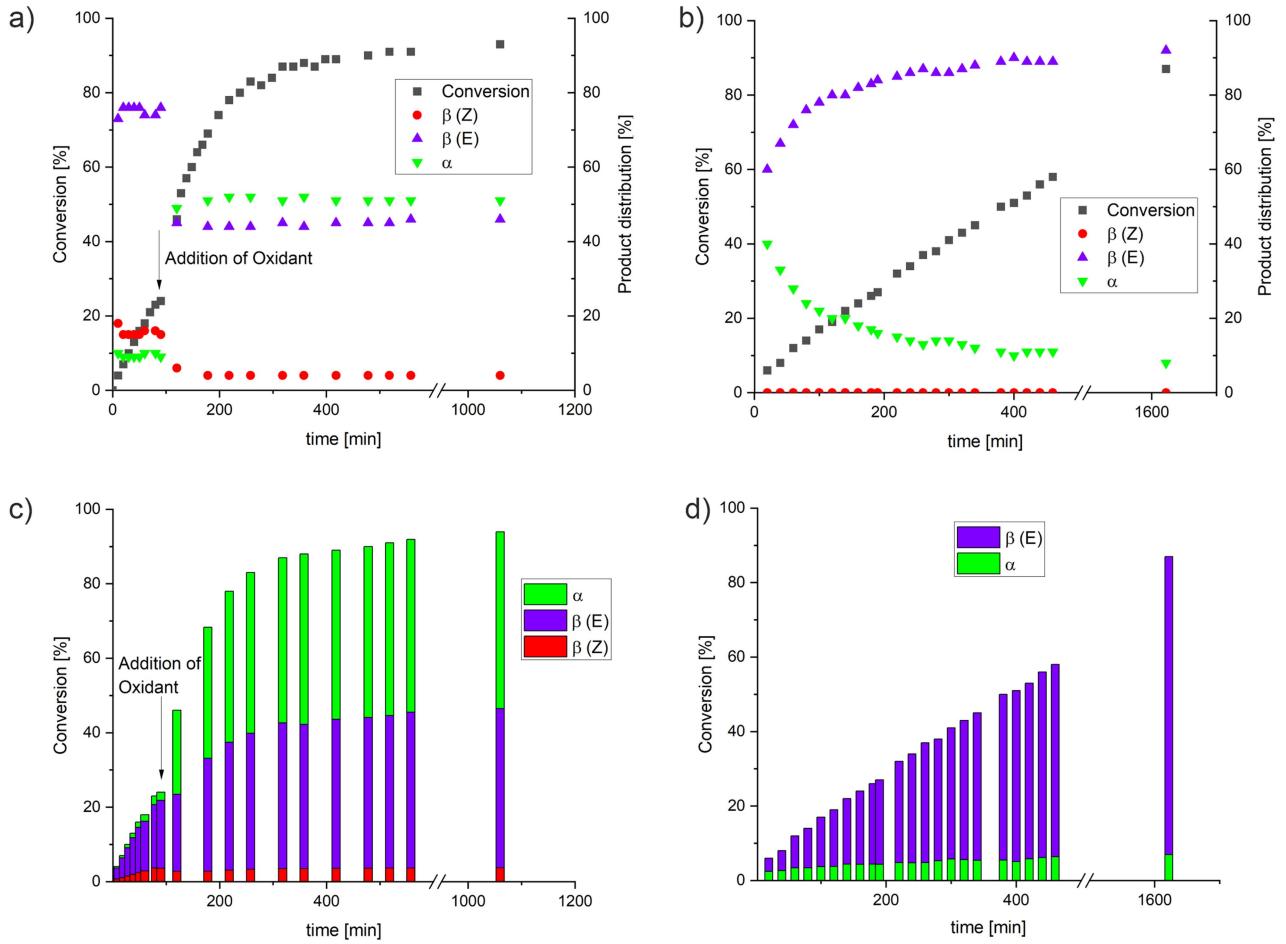

Figure 8. Conversion and product distribution plots for the hydrosilylation of hex-1-yne with Et_3SiH and 1 mol% [**L1**Rh(cod)Cl] (**3**; cf. Scheme 5). a) Addition of the oxidant $[CpFe(C_5H_4COMe)][SbF_6]$ after 90 min and b) the corresponding bar graph. c) In the presence of one equiv. of $[H(OEt_2)_2][Al(OC(CF_3)_3)_4]$ and d) the corresponding bar graph. For further experimental details, see the Supporting Information.

$\Delta TEP = +21\ cm^{-1}$. Upon addition of decamethyl ferrocene, the intensity of the band is drastically reduced, which underlines the reversibility of the redox process. To further support this finding, we reacted **1** with an oxidant in situ in an NMR tube and, subsequently, with Fc*, which refurnishes the original NMR of **1** (Figure S56).

To demonstrate the influence on reactivity of the metal complexes by applying oxidation or protonation events, we decided to investigate the rhodium-catalysed hydrosilylation of alkynes (Scheme 5). Our research group has already demonstrated that redox-switching of rhodium complexes with [1]-phosphaferrocenophanes has a profound influence on the rate of the reaction and the selectivity.[4] We have particularly chosen this rather "slow" catalytic system in order to obtain unaffected results by polymerization reactions, which are known for similar catalytic systems. When the rhodium complex [**L1**Rh(cod)Cl] (**3**) was employed as precatalyst for the conversion of 1-hexyne with triethyl silane (Table 4, entry 1), the β(*E*) and β(*Z*) isomers were found to be the main products, as expected (Figure S51). Although the addition of a proton source (entry 2) does not influence the total rate of conversion, it drastically influences

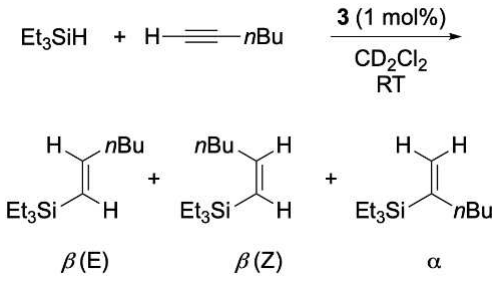

Scheme 5. Catalytic hydrosilylation of hex-1-yne with triethyl silane using [**L1**Rh(cod)Cl] (**3**) as precatalyst.

the selectivity, that is, only the β(*E*) isomer, together with a small amount of the α isomer, is formed.

From the more detailed conversion plots in Figure 8c,d it can be seen that the α isomer represents a considerable part of the initial product distribution in the beginning of the reaction. However, after a short initialization period, the β(*E*) isomer is formed (almost) exclusively, which might be attributed to, for example, conformational changes, steric effects, or coordinative

Table 4. Conversion and product distribution of the catalytic hydrosilylation of hex-1-yne with triethyl silane at room temperature. Catalyst loading (**3**): 1 mol%.

Additive[a]	*t* [min]	Conversion[b] [%]	β(*E*) :β(*Z*) :α[c]
none	480	65	70:20:10
$[H(OEt_2)_2][Al(OC(CF_3)_3)_4]$	480	64	92: < 1:7
$[CpFe(C_5H_4COMe)][SbF_6]$	240	83	45: < 1:55

[a] Additive loading of 1 mol%. [b] Conversion and yields were determined by ^{1}H NMR spectroscopy by integrating against $(SiMe_3)_2O$ as internal standard. [c] The isomers were identified from their respective coupling constants.

influences of the allylic products. When the catalyst was used without additives and a proton source was added after 90 minutes, the total amount of α and β(*Z*) isomers did not change, which shows that the change in product distribution upon protonation can indeed be attributed to a different selectivity and not to isomerization processes. By contrast, oxidation leads to a strong increase of the conversion rate (Table 4, entry 3, and Figure 8a). Again, only small amounts of the β(*Z*) isomer are observed, while the main products are the β(*E*) and α isomers. These results for the oxidized catalysts are in line with previously reported studies from our group, where addition of an oxidant leads to an increase in reactivity along with increased formation of the β(*E*) and α isomers.[4] In contrast to the protonated catalyst, this observation can definitely be attributed to isomerization. When the catalyst was used without additives and an oxidant was added after 90 minutes, the (small) amount of β(*Z*) isomer remained constant and did not change over the course of the reaction. However, the distribution of the α and β(*E*) isomers immediately changed to the ratio observed at the end of the catalysis, which demonstrates that the two isomers are in a thermal equilibrium (Figure 8a/b). As a proof of concept, we were thus able to show that both triggers act orthogonally, that is, they influence either the rate of conversion and/or the product distribution.

Overall, we report the synthesis of a novel type of redox-active and proton-sensitive phosphine ligand in which the donating capabilities can be switched orthogonally and reversibly by either protonation or oxidation. Structures of all ligands and their complexes were investigated by X-ray diffractometry and NMR spectroscopy. The influence of protonation and coordination of a metal fragment on the redox behaviour was investigated by cyclic voltammetry, showing the sensitivity of the ferrocene moiety towards changes in the ligand system. Generally speaking, switching ligand properties in situ can greatly influence the reactivity and the selectivity of coordinated metals in catalysis. As a proof of concept, the rhodium(I) complex **3** reported in this study was applied as precatalyst in hydrosilylation reactions of 1-hexyne. When the different switches were applied, they influenced either the rate of conversion and/or the product distribution. We believe that this case study demonstrates that such orthogonally multiresponsive ligands allow for fine tuning of catalytic systems, and improve control in multimetallic catalysis.[21] Further investigations in this area are currently being performed in our group.

Acknowledgements

We acknowledge financial support from the DFG-funded Transregional Collaborative Research Center SFB/TRR 88 "Cooperative effects in homo- and heterometallic complexes (3MET)" (project B4). P.M. and F.D. acknowledge financial support from the DFG (SFB 858 and Emmy Noether program DI 2054/1-1). Open Access funding enabled and organized by Projekt DEAL.

Conflict of Interest

The authors declare no conflict of interest.

Keywords: bimetallic complexes · cooperative effects · ferrocenophane · metalloligands · stimuli-responsive ligands

[1] a) O. R. Luca, R. H. Crabtree, *Chem. Soc. Rev.* **2013**, *42*, 1440–1459; b) V. Lyaskovskyy, B. de Bruin, *ACS Catal.* **2012**, *2*, 270–279; c) L. A. Berben, B. de Bruin, A. F. Heyduk, *Chem. Commun.* **2015**, *51*, 1553–1554; d) V. Blanco, D. A. Leigh, V. Marcos, *Chem. Soc. Rev.* **2015**, *44*, 5341–5370; e) K. Arumugam, C. D. Varnado Jr., S. Sproules, V. M. Lynch, C. W. Bielawski, *Chem. Eur. J.* **2013**, *19*, 10866–10875; f) J. Choudhury, *Tetrahedron Lett.* **2018**, *59*, 487–495; g) C. Ruiz-Zambrana, A. Gutiérrez-Blanco, S. Gonell, M. Poyatos, E. V. Peris, *Angew. Chem. Int. Ed.* **2021**, *60*, 20003–20011; *Angew. Chem.* **2021**, *133*, 20156–20164; h) P. Pandey, P. Daw, N. U. Din Reshi, K. R. Ehmann, M. Hölscher, W. Leitner, J. K. Bera, *Organometallics* **2020**, *39*, 3849–3863; i) M. Kaur, N. U. Din Reshi, K. Patra, A. Bhattacherya, S. Kunnikuruvan, J. K. Bera, *Chem. Eur. J.* **2021**, *27*, 10737–10748.

[2] a) C. A. Tolman, *Chem. Rev.* **1977**, *77*, 313–348; b) D. J. Nelson, S. P. Nolan, *Chem. Soc. Rev.* **2013**, *42*, 6723–6753.

[3] E. L. Rosen, C. D. Varnado, A. G. Tennyson, D. M. Khramov, J. W. Kamplain, D. H. Sung, P. T. Cresswell, V. M. Lynch, C. W. Bielawski, *Organometallics* **2009**, *28*, 6695–6706.

[4] A. Feyrer, M. K. Armbruster, K. Fink, F. Breher, *Chem. Eur. J.* **2017**, *23*, 7402–7408.

[5] L. Hettmanczyk, L. Suntrup, S. Klenk, C. Hoyer, B. Sarkar, *Chem. Eur. J.* **2017**, *23*, 576–585.

[6] For further readings on redox switchable NHCs: Y. Ryu, G. Ahumada, C. W. Bielawski, *Chem. Commun.* **2019**, *55*, 4451–4466.

[7] a) M. Abubekerov, V. Vlček, J. Wei, M. E. Miehlich, S. M. Quan, K. Meyer, D. Neuhauser, P. L. Diaconescu, *iScience* **2018**, *7*, 120–131; b) M. Abubekerov, S. M. Shepard, P. L. Diaconescu, *Eur. J. Inorg. Chem.* **2016**, 2634–2640; c) A. B. Biernesser, K. R. Delle Chiaie, J. B. Curley, J. A. Byers, *Angew. Chem. Int. Ed.* **2016**, *55*, 5251–5254; *Angew. Chem.* **2016**, *128*, 5337–5340; d) E. M. Broderick, N. Guo, T. Wu, C. S. Vogel, C. Xu, J. Sutter, J. T. Miller, K. Meyer, T. Cantat, P. L. Diaconescu, *Chem. Commun.* **2011**, *47*, 9897–9899; e) L. A. Brown, J. L. Rhinehart, B. K. Long, *ACS Catal.* **2015**, *5*, 6057–6060; f) R. Dai, P. L. Diaconescu, *Dalton Trans.* **2019**, *48*, 2996–3002; g) C. K. A. Gregson, I. J. Blackmore, V. C. Gibson, N. J. Long, E. L. Marshall, A. J. P. White, *Dalton Trans.* **2006**, 3134–3140; h) C. K. A. Gregson, V. C. Gibson, N. J. Long, E. L. Marshall, P. J. Oxford, A. J. P. White, *J. Am. Chem. Soc.* **2006**, *128*, 7410–7411; i) J. M. Kaiser, B. K. Long, *Coord. Chem. Rev.* **2018**, *372*, 141–152; j) A. Lai, Z. C. Hern, P. L. Diaconescu, *ChemCatChem* **2019**, *11*, 4210–4218; k) M. Y. Lowe, S. Shu, S. M. Quan, P. L. Diaconescu, *Inorg. Chem. Front.* **2017**, *4*, 1798–1805; l) M. Qi, Q. Dong, D. Wang, J. A. Byers, *J. Am. Chem. Soc.* **2018**, *140*, 5686–5690; m) S. M. Quan, X. Wang, R. Zhang, P. L. Diaconescu, *Macromolecules* **2016**, *49*, 6768–6778; n) S. M. Quan, J. Wei, P. L. Diaconescu, *Organometallics* **2017**, *36*, 4451–4457; o) X. Wang, A. Thevenon, J. L. Brosmer, I. Yu, S. I. Khan, P. Mehrkhodavandi, P. L. Diaconescu, *J. Am. Chem. Soc.* **2014**, *136*, 11264–11267; p) J. Wei, P. L. Diaconescu, *Acc. Chem. Res.* **2019**, *52*, 415–424; q) J. Wei, M. N. Riffel, P. L. Diaconescu, *Macromolecules* **2017**, *50*, 1847–1869.

[8] E. M. Broderick, N. Guo, C. S. Vogel, C. Xu, J. Sutter, J. T. Miller, K. Meyer, P. Mehrkhodavandi, P. L. Diaconescu, *J. Am. Chem. Soc.* **2011**, *133*, 9278–9281.

[9] a) Y. Shen, S. M. Shepard, C. J. Reed, P. L. Diaconescu, *Chem. Commun.* **2019**, *55*, 5587–5590; b) S. Ibáñez, M. Poyatos, L. N. Dawe, D. Gusev, E. Peris, *Organometallics* **2016**, *35*, 2747–2758.
[10] a) E. Deck, H. E. Wagner, J. Paradies, F. Breher, *Chem. Commun.* **2019**, *55*, 5323–5326; b) A. Feyrer, F. Breher, *Inorg. Chem. Front.* **2017**, *4*, 1125–1134.
[11] I. M. Lorkovic, R. R. Duff, M. S. Wrighton, *J. Am. Chem. Soc.* **1995**, *117*, 3617–3618.
[12] a) A. T. Biju, K. Hirano, R. Fröhlich, F. Glorius, *Chem. Asian J.* **2009**, *4*, 1786–1789; b) L. Benhamou, V. César, H. Gornitzka, N. Lugan, G. Lavigne, *Chem. Commun.* **2009**, 4720–4722.
[13] P. Mehlmann, F. Dielmann, *Chem. Eur. J.* **2019**, *25*, 2352–2357.
[14] B. M. Neilson, V. M. Lynch, C. W. Bielawski, *Angew. Chem. Int. Ed.* **2011**, *50*, 10322–10326; *Angew. Chem.* **2011**, *123*, 10506–10510.
[15] a) S. Gaikwad, A. Goswami, S. De, M. Schmittel, *Angew. Chem. Int. Ed.* **2016**, *55*, 10512–10517; *Angew. Chem.* **2016**, *128*, 10668–10673; b) J. Choudhury, S. Semwal, *Synlett* **2018**, *29*, 141–147.
[16] R. H. Crabtree, *New J. Chem.* **2011**, *35*, 18–23.
[17] M. Neel, P. Retailleau, A. Voituriez, A. Marinetti, *Organometallics* **2018**, *37*, 797–801.
[18] Recent reviews on sandwich compounds: a) D. E. Herbert, U. F. J. Mayer, I. Manners, *Angew. Chem. Int. Ed.* **2007**, *46*, 5060–5081; *Angew. Chem.* **2008**, *119*, 5152–5173; b) M. Tamm, *Chem. Commun.* **2008**, 3089–3100; c) H. Braunschweig, T. Kupfer, *Acc. Chem. Res.* **2010**, *43*, 455–465; d) H. Bhattacharjee, J. Müller, *Coord. Chem. Rev.* **2016**, *314*, 114–133.
[19] a) A. N. Nesmejanow, W. A. Ssasonowa, V. N. Drosd, *Chem. Ber.* **1960**, *93*, 2717–2729; b) M. Herberhold, H.-D. Brendel, *J. Organomet. Chem.* **1993**, *458*, 205–209; c) I. Noviandri, K. N. Brown, D. S. Fleming, P. T. Gulyas, P. A. Lay, A. F. Masters, L. Phillips, *J. Phys. Chem. B.* **1999**, *103*, 6713–6722.
[20] a) P. Zanello, *Inorganic Electrochemistry: Theory, Practice and Application*, RSC, Cambridge, **2003**; b) B. Neumann, U. Siemeling, H.-G. Stammler, U. Vorfeld, J. G. P. Delis, P. W. N. M. van Leeuwen, K. Vrieze, J. Fraanje, K. Goubitz, F. Fabrizi de Biani, *J. Chem. Soc. Dalton Trans.* **1997**, 4705–4712.
[21] R. Maity, B. S. Birenheide, F. Breher, B. Sarkar, *ChemCatChem* **2021**, *13*, 2337–2370.
[22] Deposition Numbers 2087629 (for **L1**), 2087627 (for **L2**), 2087628 (for **1**), 2087630 (for **2**), 2087635 (for **3**), 2087632 (for **4**), 2087636 (for **5**), 2087631 (for **6**), 2087633 (for **L1H+**), 2087634 (for **2H+**) contain the supplementary crystallographic data for this paper. These data are provided free of charge by the joint Cambridge Crystallographic Data Centre and Fachinformationszentrum Karlsruhe Access Structures service.

Manuscript received: June 4, 2021
Accepted manuscript online: August 30, 2021
Version of record online: September 6, 2021

